Numerical Simulation of Typhoon Gladys (1994) and Its Interaction with Taiwan Terrain Using the GFDL Hurricane Model

CHUN-CHIEH WU

Department of Atmospheric Sciences, National Taiwan University, Taipei, Taiwan

(Manuscript received 30 December 1999, in final form 24 October 2000)

ABSTRACT

Numerical integrations using the Geophysical Fluid Dynamics Laboratory (GFDL) hurricane model were performed to study the evolution of Typhoon Gladys (1994) and its interaction with the Taiwan terrain. Consistent with most previous studies, the Taiwan topography results in the deceleration of Gladys's translation speed and southward deviation as it approaches Taiwan. On the other hand, Gladys accelerates northwestward while passing Taiwan, which is likely to be related to the moist processes, and differs from the track pattern in the dry model of Lin et al. Although the GFDL hurricane model forecast underestimates Gladys's intensity, the model can capture the evolution of Gladys's intensity, especially its weakening during landfall, which is primarily due to the cutoff of the water vapor supply in the boundary layer as Gladys approached the Taiwan terrain. Other mesoscale phenomena, including the pattern of heavy precipitation and the formation of secondary lows, are well simulated by the model, though their locations are somewhat different from those observed. Detailed analyses indicate that the surface low pressure center to the east of the Central Mountain Range (CMR) is induced by the downslope adiabatic warming (foehn) associated with the circulation of Gladys. The quasi-stationary secondary low to the west of the CMR is mainly induced by the environmental easterly flow over the CMR, while the downslope adiabatic warming associated with the circulation of Gladys acts to enhance it as Gladys is close to Taiwan. The potential vorticity budget analysis indicates that the condensational heating plays a major role in the potential vorticity evolution around the storm, while the surface frictional dissipation of the potential vorticity becomes more significant as Gladys is over the Taiwan terrain. Finally, the experiment with a larger and stronger initial typhoon vortex indicates that different initial specification of a typhoon vortex can result in a different track pattern and thus leads to a totally different typhoon–topography interaction, suggesting the importance of typhoon initialization for storm prediction near Taiwan.

1. Introduction

Of the natural disasters occurring in Taiwan, tropical cyclones are the most serious meteorological phenomenon. On average, three or four typhoons occur annually. The strong winds and heavy precipitation associated with a typhoon significantly affect the weather in Taiwan, even if the storm does not make landfall. Significant variations in track and intensity occur as a typhoon approaches the island. This is due to the high altitude and complicated mesoscale topography of Taiwan's Central Mountain Range (CMR), which has an average elevation of more than 2000 m (while the highest peak is close to 4000 m), and dimensions of 300 km by 100 km.

The interaction of the typhoon circulation with the CMR also produces significant mesoscale variations in pressure, wind, and precipitation distribution over Taiwan (Wang 1980, 1989). For example, mesoscale secondary low centers can form on the lee side of the CMR and may develop into a new tropical cyclone, replacing the original storm. The track deflection, the development of secondary lows, the changes in intensity, and the mesoscale structure of pressure, wind, and precipitation associated with an approaching typhoon make the forecasting of a tropical cyclone approaching Taiwan an extremely difficult task. Understanding the dynamics of typhoon circulation and its interaction with the Taiwan terrain, and the forecasting of track, intensity, mesoscale wind, and precipitation distribution, are some of the most important scientific and forecasting problems for meteorologists in Taiwan (Wu and Kuo 1999).

In addition to some insightful theoretical studies on the dynamics of flow over topography (Smith 1979, 1980, 1989; Smolarkiewicz and Rotunno 1989; Schar and Smith 1993a,b; Peng et al. 1995; Smith and Smith 1995; Schar and Durran 1997; Rotunno et al. 1999), progress in understanding the dynamics of typhoon circulation and its interaction with the Taiwan topography has been made in the past two decades through various observational studies (Brand and Blelloch 1974; Wang

Corresponding author address: Dr. Chun-Chieh Wu, Department of Atmospheric Sciences, National Taiwan University, 61, Ln. 144, Sec. 4, Keelung Rd., Taipei 10772, Taiwan.
E-mail: cwu@typhoon.as.ntu.edu.tw

1980, 1989; Shieh et al. 1996) and idealized numerical simulations (Chang 1982; Bender et al. 1985, 1987; Yeh and Elsberry 1993a,b; Sun and Chern 1994; Huang and Lin 1997; Huang and Hsu 1998; Lin et al. 1999). However, many details of such an interaction are still not well understood, mainly due to major limitations both from the lack of mesoscale observations that may provide a detailed description of the storms as they move across the island of Taiwan, and from the lack of high-resolution mesoscale model simulations that may offer insights into the mesoscale processes responsible for the structural changes associated with the interaction of a typhoon with the mesoscale topography.

While most previous studies have either focused on the observational analyses or numerical simulation under an idealized environment, there is a lack of information on the synergy between the observational and modeling work, and the interplay between real-case numerical models and mesoscale analysis. As a first step toward adopting the above approach, in this study, we used a well-developed typhoon model, that is, the Geophysical Fluid Dynamics Laboratory (GFDL) hurricane prediction system (Kurihara et al. 1995, 1998), to perform a real-case simulation of Typhoon Gladys (1994). [Note that the finest horizontal resolution of $\frac{1}{6}^\circ$ in the current study is much higher than the 60-km resolution used in Chang (1982) and the 45-km resolution in in Yeh and Elsberry (1993a,b), and the use of 18 levels in sigma coordinates is also much better than the 11 levels used in Bender et al. (1987). Therefore the current work should have the capability to resolve a more detailed terrain feature and boundary layer flow field.] Results are compared with observations to evaluate the capability of the model simulation. The effect of the Taiwan terrain on the evolution of Gladys is also investigated through different numerical experiments.

The objectives of this paper are twofold: first, to understand the model's capability in simulating the track, intensity, and mesoscale features of Gladys under the influence of the Taiwan terrain; and second, to study the physical mechanisms that affect the evolution of Gladys from various numerical experiments. It is noted that some preliminary analysis using coarse-grid (outer nest) model output has been presented by Wu et al. (1999a,b). In this paper, the focus is on the analysis of the highest-resolution (inner nest) model data, which is able to depict the detailed mesoscale structure as Gladys approached Taiwan. Section 2 describes the model design. Some observed features associated with Gladys and the model results are discussed in section 3. The summary appears in section 4.

2. Model description and experimental design

a. Model description

The model used in this case study is the GFDL hurricane prediction system (Kurihara et al. 1998). A basic summary of this system is presented here, outlining the three major components of this system, that is, model, initialization, and integration.

1) MODEL

The GFDL multiply nested movable mesh hydrostatic model originally described by Kurihara and Bender (1980) is used for the model hurricane forecasts, with additional model details presented in Tuleya et al. (1984), Bender et al. (1987), Bender et al. (1993, hereinafter BRTK), and Tuleya (1994). The model is a primitive equation model formulated in latitude, longitude, and sigma coordinates, with 18 levels in the vertical (Table 1 of Kurihara et al. 1990). The integration domain spans 75° latitude by 75° longitude, and has a triply nested grid system with resolutions of 1°, $\frac{1}{3}^\circ$, and $\frac{1}{6}^\circ$ (Table 1 of BRTK). The outermost domain extends from 10°S to 65°N in the meridional direction, and varies in the zonal direction, depending on the storm's location at each forecast time. (In the case of this study, it is fixed between 85° and 160°E in the zonal direction.)

The model physics includes a cumulus parameterization scheme described by Kurihara (1973) with some modifications (appendix C of Kurihara and Bender 1980), a Monin–Obukhov framework for the interactions at the surface, and the Mellor and Yamada (1974) level 2 turbulence closure scheme for the vertical diffusion with a background diffusion coefficient added. In addition, as described by Tuleya (1994), the Schwarzkopf and Fels (1991) infrared and Lacis and Hansen (1974) solar radiation parameterizations are incorporated, including interactive radiative effects of clouds and a diurnal radiation cycle, along with land surface temperature computed by an energy equation containing a soil layer. The sea surface temperature is specified and held fixed to the initial value throughout the integration.

2) INITIALIZATION

The initial condition for each forecast experiment is determined from the hurricane model initialization scheme described in Kurihara et al. (1993) and Kurihara et al. (1995, hereinafter KBTR). As initial input data, this scheme uses the National Centers for Environmental Prediction (NCEP) T126 global analysis, as well as the tropical cyclone message file containing the specific storm location, intensity, and structure information. Using a simple smoothing technique (as described in BRTK), the flow field is separated into a mean and disturbance component. The region (r_0; 700 km in this study) containing the hurricane vortex resolved in the NCEP global analysis is identified in the disturbance field. Using an optimal interpolation and merging scheme, the background environmental field is reconstructed across the region r_0, while the flow field outside of the storm domain remains unchanged. According to KBTR, this technique successfully removes the hurri-

TABLE 1. Summary of numerical experiments.

Expt	Topography	Bogusing	Environmental flow
B	U.S. Navy's global topography dataset	Gladys-like vortex	Environmental flow field using the GFDL initializatin process
NT	Same as above, but excluding Taiwan terrain	Same as above	
NB	U.S. Navy's global topography dataset	None	
B2	Same as above	Gladys-like vortex, but with stronger intensity and larger size	

cane disturbance in the global analysis within the r_0 region, while retaining most of the important environmental flow structure.

In the next step of the initialization system by KBTR, both symmetric and asymmetric components of the specified vortex are generated. First, an axisymmetric version of the GFDL hurricane model is integrated such that the tangential wind is forced toward a target flow field that resembles the observed hurricane wind profile obtained from the tropical cyclone message, which is distributed by the Joint Typhoon Warning Center (JTWC). Second, by using the tangential wind distribution obtained as input, a simplified version of a barotropic model (Ross and Kurihara 1992) is run in order to estimate the asymmetric flow due to the beta gyre (pair of vortices produced from the advection of planetary vorticity). The combination of the axisymmetric and asymmetric flow fields generates a hurricane vortex that has a much higher resolution than the vortex in the original global analysis and is consistent with the GFDL model. It is reinserted into the environmental flow field in the correct position to produce the initial wind and moisture field. A static initialization is then employed to recover the mass field. KBTR demonstrated improvement in the performance of the GFDL hurricane model forecasts using this approach.

3) INTEGRATION

The integration for each simulation was run for 72 h using the lateral boundary values specified from the forecasts of the NCEP global spectral model, linearly interpolated in time to hourly values (Kurihara et al. 1989).

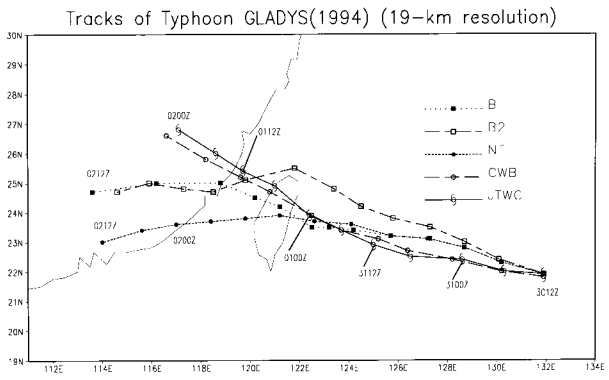

FIG. 1. Tracks for Typhoon Gladys (1994) from JTWC and CWB analyses, and the model simulations (B, NT, B2) for every 6 h.

b. Experimental design

To understand the evolution of Gladys and the effect of the Taiwan topography on Gladys, four 72-h model integrations (see Table 1) were performed, starting at 1200 UTC 30 August 1994. The first experiment made a 72-h forecast using the GFDL hurricane prediction system with a bogus vortex for Gladys based on the storm message from JTWC. This experiment can be regarded as the control experiment (referred to as expt B), and also as a forecast since it was integrated based on information available at the starting time. The second simulation (referred to as expt NT) excludes the Taiwan topography to show the impact of the Taiwan terrain on Gladys (linear extrapolation was done at points under the terrain, while hydrostatic relation is kept to obtain the new surface pressure). The third one (referred to as expt NB) removes the bogus vortex to indicate the evolution of the environmental flow presuming Gladys did not exist. The fourth one (referred to as expt B2) contains a bogus vortex with stronger intensity (initial maximum wind speed of 60 kt compared to 50 kt in expt B) and larger size (initial radius of gale force winds of 200 km compared to 100 km in expt B) to study the sensitivity of the model simulation, as well as the terrain impact, under different typhoon strengths.

3. Results

a. Synopsis of Gladys

Typhoon Gladys was the 16th typhoon in the western North Pacific in 1994. The disturbance was named a tropical depression at 0000 UTC 22 August near 24°N, 175°E. After 23 August, Gladys moved westward along the southern edge of a subtropical ridge and began to intensify. According to the official report of the Central Weather Bureau (CWB), Gladys was upgraded to a tropical storm at 0600 UTC 24 August, and reached its maximum intensity at 0000 UTC 1 September with an estimated maximum surface wind of 65 kt (see Figs. 1 and 2 on track and intensity analysis). It made landfall at Su-Au, Taiwan, at about 0250 UTC 1 September, and left Taiwan near Hsin-Chu at 0600 UTC on the same day. Gladys weakened considerably while approaching and crossing the northern half of Taiwan. After passing

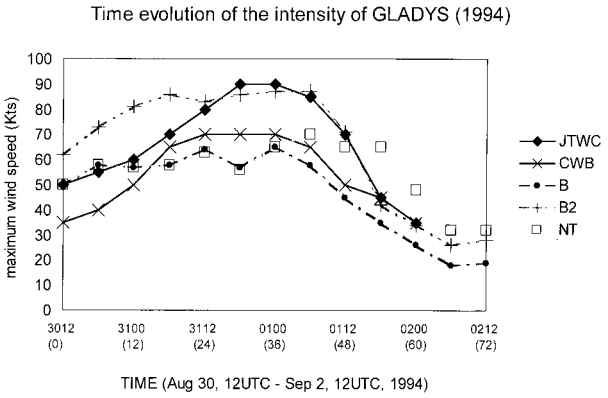

FIG. 2. Maximum surface wind (in kt) for Gladys (1994) as function of time (at 6-h interval) from JTWC and CWB analyses, and the model simulations (B, NT, B2).

Taiwan, Gladys turned toward the west-northwest, tracked inland over mainland China, and gradually dissipated over land.

Between Gladys's landfall at 0250 UTC and departure at 0600 UTC on the same day, the sea-level pressure and surface temperature around Taiwan decreased considerably. As to precipitation, major rainfall occurred in northeastern Taiwan and over the mountainous area, which Gladys passed over. Data from the surface station show that there was a local low near southwestern Taiwan [Fig. 3; also see Fig. 4 in Wu et al. (1999a)]. Another interesting feature observed was a local low (Fig. 3) near southeastern Taiwan, which did not build up until a few hours before Gladys made landfall on Taiwan. During this period, the temperature in southeast Taiwan remained at about 30°C, and the relative humidity was 30% lower than other areas in Taiwan. This appears to be the so-called foehn, which was induced by the adiabatic warming after the flow associated with Gladys crossed over the mountains. This point will be further examined in the next section.

b. The control experiment

1) SYNOPTIC FEATURES

Figure 1 shows the comparison of forecast track with the best track analyses from both the CWB and the JTWC. In general, the analyses between CWB and JTWC are in agreement with each other. The control numerical experiment shows a fairly accurate track simulation for Gladys, especially in the first 54 h, though the model storm moves too slowly between about 27 and 39 h. The position error compared to that of the JTWC analysis is 82 and 151 km for the 24- and 48-h forecasts, respectively. The model storm in experiment B slows down between 27 and 39 h compared with the observed storm position, makes landfall at 46 h, and leaves Taiwan at 51 h, compared with the observed times of 39 and 42 h, respectively. This error may be

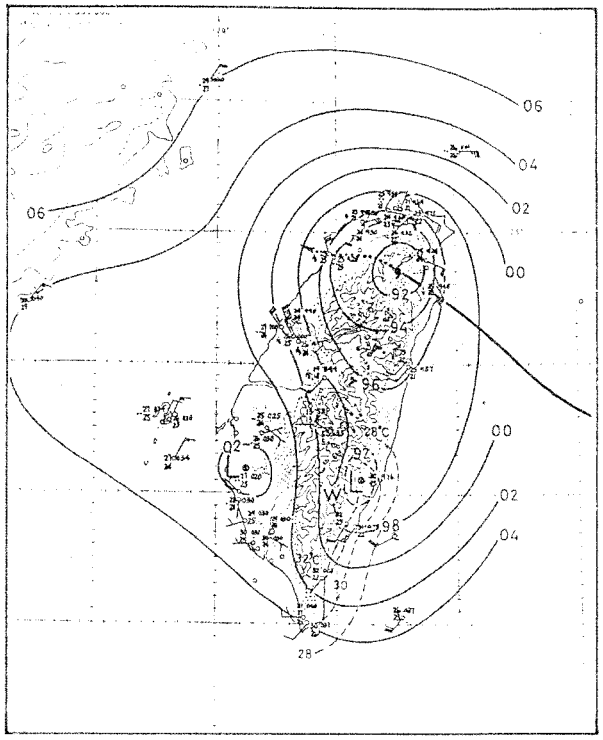

FIG. 3. Surface map with sea surface pressure (contour interval of 2 mb) at 0004 UTC 31 Aug 1994. Track for Typhoon Gladys (1994) is also indicated. [After Wu et al. (1999a).]

in part related to the inaccurate prognosis of the large-scale environmental flow upstream of the high terrain, and in part due to the incorrect storm structure such as the vertical extent of the vortex. After 54 h, the model storm of experiment B turns westward while the best track continued northwestward, and the position error at 72 h increases to 350 km. The analysis of the simulated deep-layer (850–200 mb) mean flow indicates that the track of Gladys agrees very well with the deep-layer mean flow at 24 and 42 h (Figs. 4a and 4b), but not very well at 60 h (Fig. 4c). Since the vertical extent of Gladys became much shallower after passing over Taiwan, instead of using the deep-layer mean wind, we also examine the steering flow as defined by the lower- to middle-level (850–500 mb) mean flow (Fig. 4d). It is shown that the lower- to middle-level mean flow agrees reasonably well with the storm motion. This result is consistent with Dong and Neumann (1986), indicating that the height of the best steering level or the depth of the best deep-layer steering should increase in proportion to storm intensity. This concept is practically useful for predicting storms over topography when their intensities and structures undergo dramatic changes. The mean flow analysis also indicates that after Gladys departs Taiwan, the high pressure center over China (Fig. 4d) is located to the west of the observed center, causing the model track to deviate to the south of the best track.

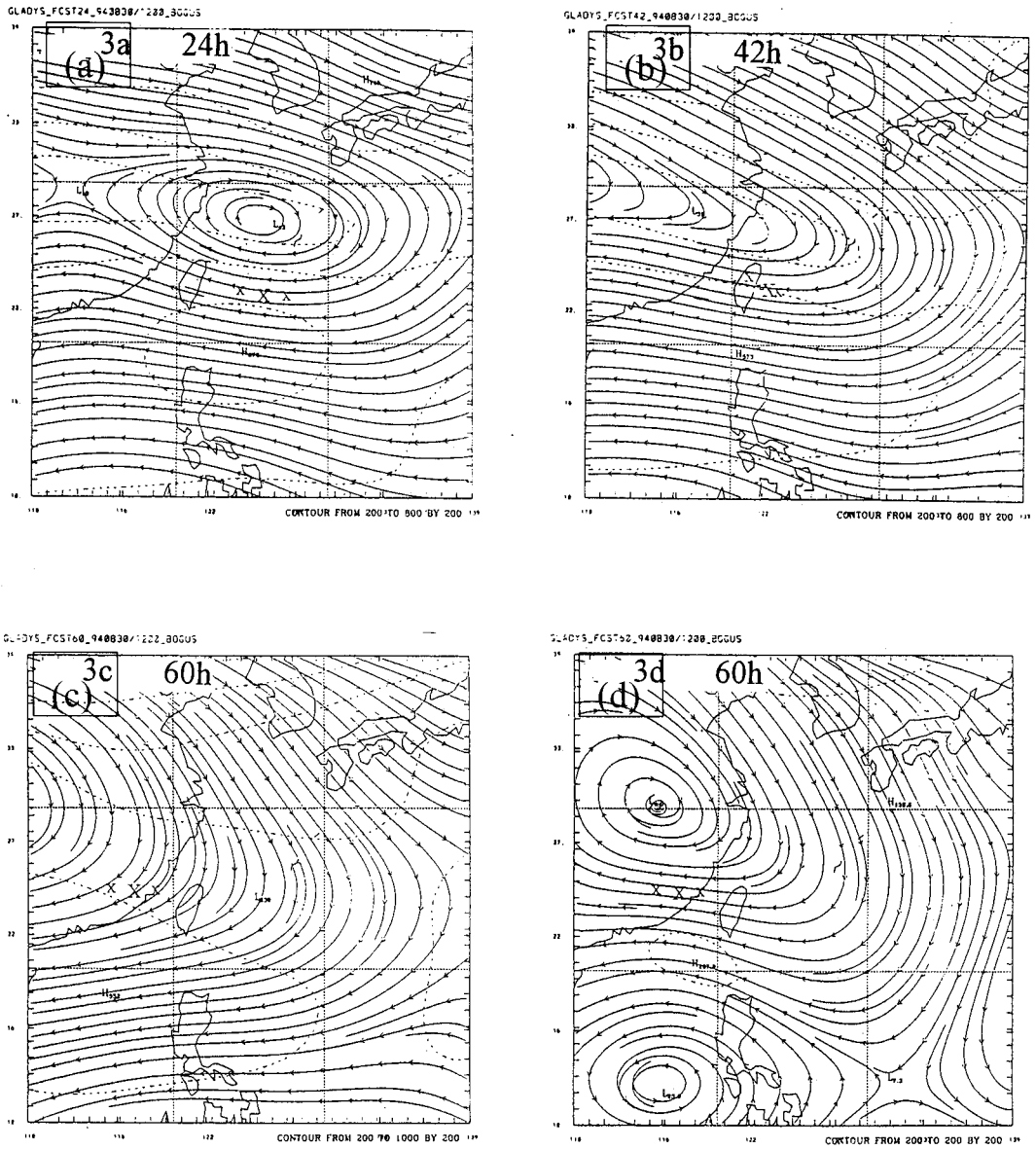

FIG. 4. The simulated streamlines of the deep-layer (850–200 mb) mean wind at (a) 24, (b) 42, and (c) 60 h. (d) Same as in (c) but for lower- to midlayer (850–500 mb) mean wind. The locations of Gladys at each time, 6 h earlier and 6 h later, are indicated as ×'s.

As to the intensity forecast, the comparisons of the maximum surface wind with the analyses from both the CWB and the JTWC are shown in Fig. 3. Both the CWB and JTWC analyses show that Gladys reached its maximum intensity at 0000 UTC 1 September [about 10 h before landfall, which is consistent with the statistics of 12 h from Brand and Blelloch (1974) and the result of 10 h from the idealized simulation with a 5 m s^{-1} background wind in Bender et al. (1987)]. Yet a large difference exists between the two analyses. For example, as Gladys reaches its maximum intensity, the maximum surface wind speed indicated by the analysis from the JTWC (85 kt) is 30% higher than that from the CWB (65 kt). This difference results in part from the different definition of the surface wind (i.e., the JTWC uses the 1-min-average wind, while the CWB uses the 10-min-average wind). Although the GFDL hurricane model forecast underestimates Gladys's intensity throughout the forecast period, the model can capture the evolution of Gladys's intensity, especially the weakening during landfall. Nevertheless, as the intensity of a typhoon is affected by large and complex arrays of physical processes governing the interaction of the storm (both the eyewall and mesoscale dynamics) with the underlying ocean and the atmospheric environment, the uncertainty of the intensity prediction remains a big challenge for

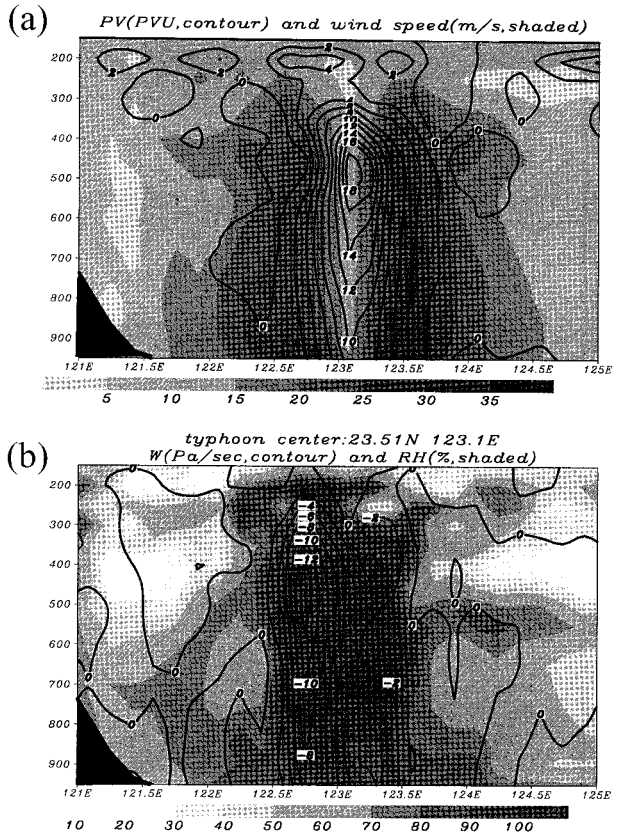

FIG. 5. West–east cross section, cutting through the storm center, of (a) potential vorticity (contour interval of 2 PVU) and horizontal wind speed (unit of m s^{-1}, shaded), and (b) vertical velocity (contour interval of 2 Pa s^{-1}) and relative humidity (%, shaded) at 36 h from the control experiment (expt B). The bold solid line indicates the topography of Taiwan.

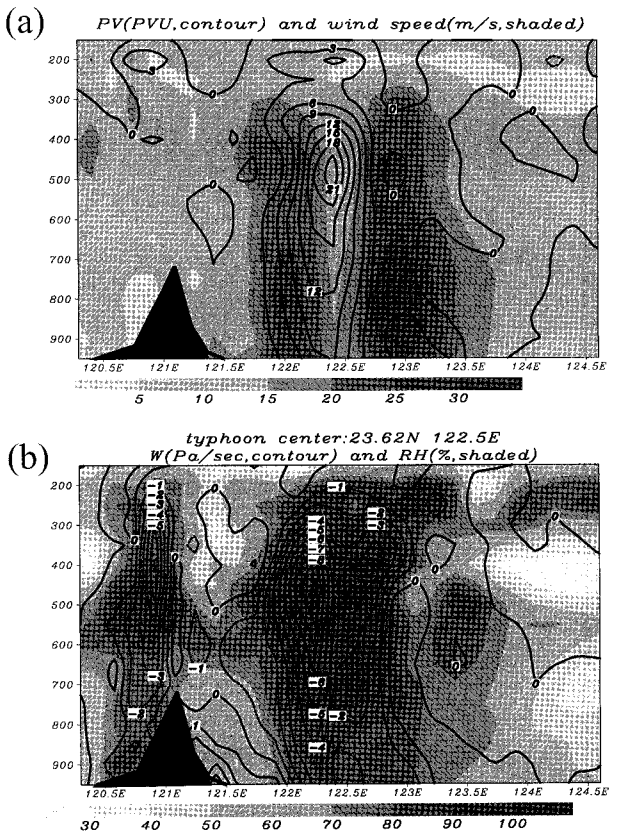

FIG. 6. West–east cross section, cutting through the storm center, of (a) potential vorticity (contour interval of 3 PVU) and horizontal wind speed (unit of m s^{-1}, shaded), and (b) vertical velocity (contour interval of 1 Pa s^{-1}) and relative humidity (%, shaded) at 42 h from the control experiment (expt B). The bold solid line indicates the topography of Taiwan.

dynamical hurricane models (Bender and Ginis 2000; Wu et al. 2000).

2) MESOSCALE STRUCTURES

(i) Gladys's structure

In this section several meteorological variables, such as the zonal cross section of potential vorticity (PV), horizontal wind, vertical velocity, temperature, and relative humidity (RH) fields are analyzed for every 6 h from 36 to 54 h, the period before and after the storm of experiment B hits Taiwan. At 36 h, high-PV air (Fig. 5a) is concentrated within the inner 2° of the storm center, and extends vertically up to about 200 mb with a PV maximum of 18 PVU (potential vorticity unit, 10^{-6} m^2 K s^{-1} kg^{-1}) at about 500 mb. The maximum horizontal wind speed (Fig. 5a) reaches 35 m s^{-1} at 900 mb on the eastern flank of the eyewall, with a region of relatively weak wind over the storm center. Though no clear subsidence motion occurs in the center, the vertical velocity distribution (Fig. 5b) displays an eyewall-like structure with asymmetric strong updrafts around the center. To the west of the storm center, a column area of strong upward velocity exists, with a maximum value of -12 Pa s^{-1} (about 1.2 m s^{-1}) at 500 mb. Comparison of Figs. 5a and 5b indicates that the maximum horizontal wind speed and the maximum vertical velocity occurs on different sides relative to the storm center. As the upward motion is partly related to the local thermodynamics (e.g., static stability) and partly to the local horizontal wind field (e.g., convergence), this may help explain why the maximum vertical velocity does not necessarily occur in the same area with maximum horizontal wind. The RH distribution (Fig. 5b) indicates that within the inner 100 km of the storm center, the air is totally saturated.

At 42 h (about 4 h before landfall), even though the maximum surface wind has decreased, a higher maximum PV of 21 PVU at 500 mb in the center and a maximum horizontal wind of 35 m s^{-1} at 850 mb to the east of the storm center (Fig. 6a) are found. However, the vertical velocity (Fig. 6b) becomes weaker with a maximum value of -8 Pa s^{-1} slightly to the west of the storm center, while the saturated air still remains

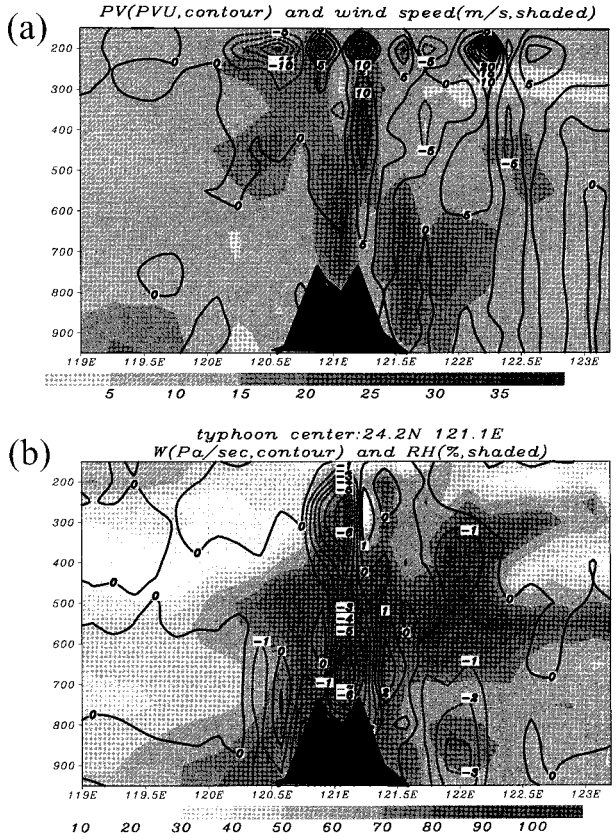

FIG. 7. West–east cross section, cutting through the storm center, of (a) potential vorticity (contour interval of 5 PVU) and horizontal wind speed (unit of m s^{-1}, shaded), and (b) vertical velocity (contour interval of 1 Pa s^{-1}) and relative humidity (%, shaded) at 48 h from the control experiment (expt B). The bold solid line indicates the topography of Taiwan.

through the troposphere near the storm center. Another interesting feature at 42 h is the presence of strong upward motion to the west of the CMR, and weak downward motion to the east of it. The upward motion to the west of the CMR appears to be associated with a local convective area over the CMR. On the other hand, the weak downward motion to the east of the CMR is associated with the cross-mountain downslope northerly wind (see Figs. 8c and 8d).

As Gladys reaches central Taiwan (48 h), the eyewall feature is still distinguishable from the distribution of the horizontal wind speed (Fig. 7a), where two wind maxima straddle the mountain (bold dark line) around the storm center. The vertical extension of the cyclonic wind shrinks due to the weakening of the storm above the mountain, while the maximum PV remains 10 PVU at 400 mb. Note that some PV noises are present around 150 mb, which are probably produced by the finite-difference scheme in calculating the PV while using 100 mb as the top level. As shown in Fig. 7b, the distribution of RH becomes less organized above the storm center, while the vertical velocity still reaches -7 Pa s^{-1}, with two peaks at 700 and 300 mb, respectively. A more detailed analysis (figure not shown) indicates that the maximum upward motion at both levels is associated with the local horizontal wind convergence at each level. After the storm passes over Taiwan (figure not shown), Gladys quickly weakens with weaker cyclonic circulation and shallow and tilted vertical extent, and the whole typhoon structure disintegrates.

(ii) The effect of Taiwan terrain on Gladys's structure

The horizontal wind vector and RH fields at $\sigma = 0.8563$ (Fig. 8a) show a clear cyclonic wind around a well-defined storm area with high RH as Gladys approaches Taiwan (36 h). However, at the model's lowest level, $\sigma = 0.995$ (Fig. 8b), a tongue of relatively low-RH air has extended to the south of the storm center in the boundary layer. This is an early sign that the drier air originating in the mountainous region of Taiwan has begun to interact with the storm circulation in the lower boundary layer. At 42 h, as Gladys moves closer to Taiwan (4 h before landfall), the storm remains well organized with saturated air in the storm center at $\sigma = 0.8563$ (Fig. 8c). However, at $\sigma = 0.995$ (Fig. 8d), a large area of downslope warm (due to adiabatic warming) and dry air (as in Lin et al. 1999) has intruded into the whole southwest quardrant of the storm. This result is consistent with the idealized simulation (e.g., expt T10) in Bender et al. (1987), which indicated that the Taiwan terrain affects the storm intensity by cutting off the water supply in the boundary layer.

(iii) The secondary lows

Regarding the formation of the secondary lows, as described in section 3a (e.g., Fig. 3), a local stationary low had persisted over southwestern Taiwan during a period of few days before and after Gladys hit Taiwan. A stationary low center (L_1) is simulated over west-central Taiwan in both experiments B (Figs. 9a and 9b for 36 and 42 h, individually) and NB (Figs. 9c and 9d), though the observed one is more to the south. When Gladys is still far away from Taiwan, the stationary low (L_1) can be explained as a response due to the environmental easterly flow over the CMR. As Gladys's circulation began to affect Taiwan, a close examination of flow field (e.g., Figs. 8a and 8b) shows that L_1 is enhanced due to the downslope adiabatic warming associated with the orographically deflected typhoon circulation. The above result from a real-case study of Gladys reveals possible mechanisms for lee vortex formation, which are consistent with the combined findings from the idealized simulations of Lin et al. (1999) for a cyclone over a bell-shaped mountain, and of Sun et al. (1991) and Lin et al. (1992) for a uniform flow over Taiwan topography.

Note that another weak low (L_2) is also simulated in

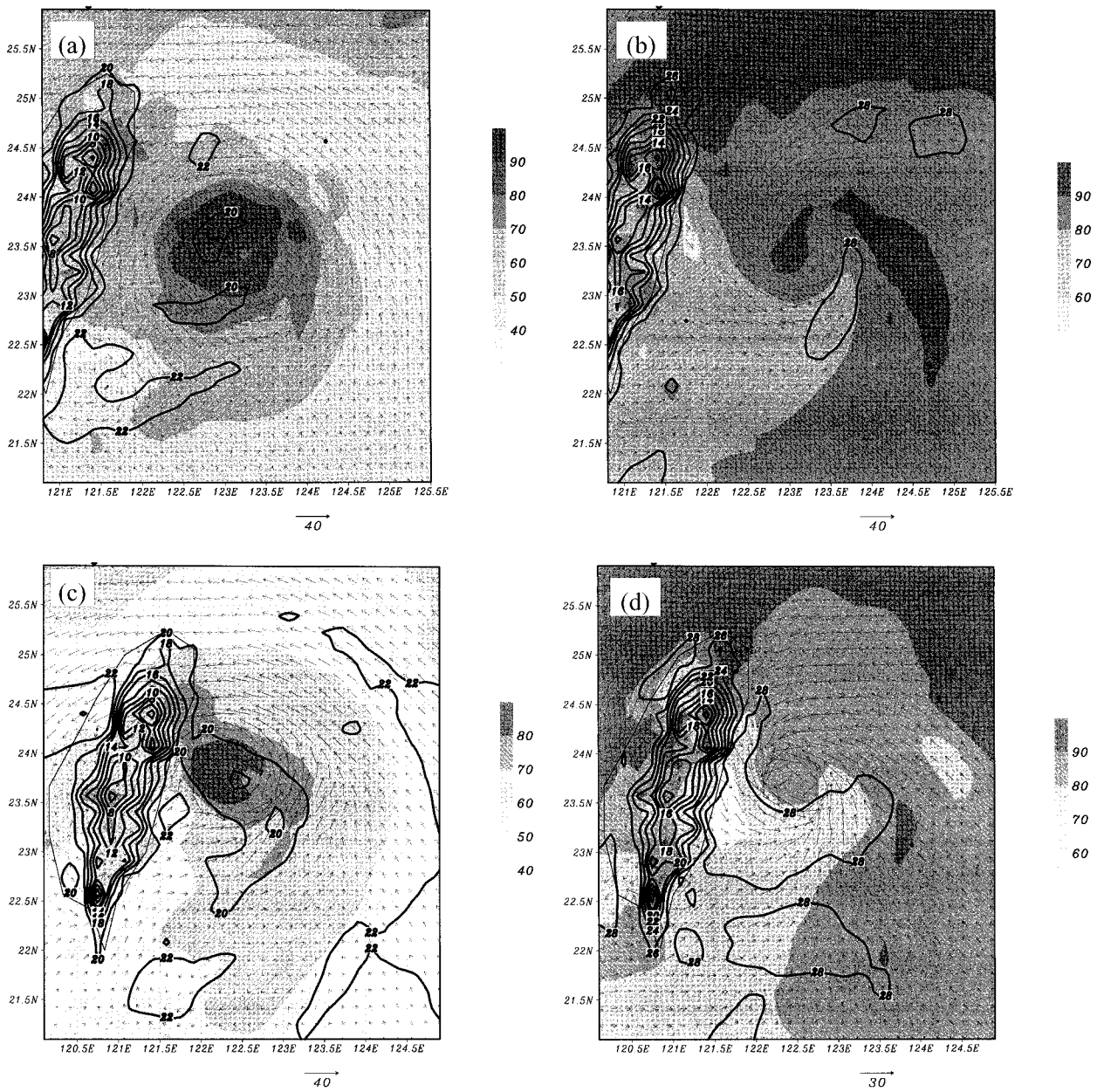

FIG. 8. Distribution of horizontal wind (in arrow), temperature (contour interval of 2°C), and relative humidity (shading with interval of 10%) at (a) $\sigma = 0.8563$ and (b) $\sigma = 0.995$ at 36 h from the control experiment (expt B); (c) and (d) same as in (a) and (b) but for 42 h.

the eastern-central part of Taiwan (Figs. 9a and 9b), and this is well in agreement with the observed feature described in section 3a (Fig. 3). As indicated in Figs. 8b–d, a local temperature maximum and RH minimum (56% for Fig. 8d) exists at the L_2 location, while the zonal cross section of vertical velocity at 42 h (Fig. 8b) indicates a region of weak downslope wind on the eastern slope of the mountain. The above temperature, RH, and vertical velocity information clearly shows that the formation of L_2 is associated with the downslope dry and warm air (foehn), which is well simulated in this model. As discussed in Shieh et al. (1996), this type of foehn phenomenon occurs quite often in the eastern-central or southeastern region of Taiwan when a typhoon moves northwestward through northern Taiwan.

(iv) The rainfall distribution

The accumulated 36–54-h precipitation from the model (Fig. 10a) is compared with that from surface observations in Fig. 10b. The shadings in Figs. 10a and 10b also indicate the Taiwan terrain resolved from the model and from the actual terrain data with 30-s resolution, respectively. Besides missing the local heavy

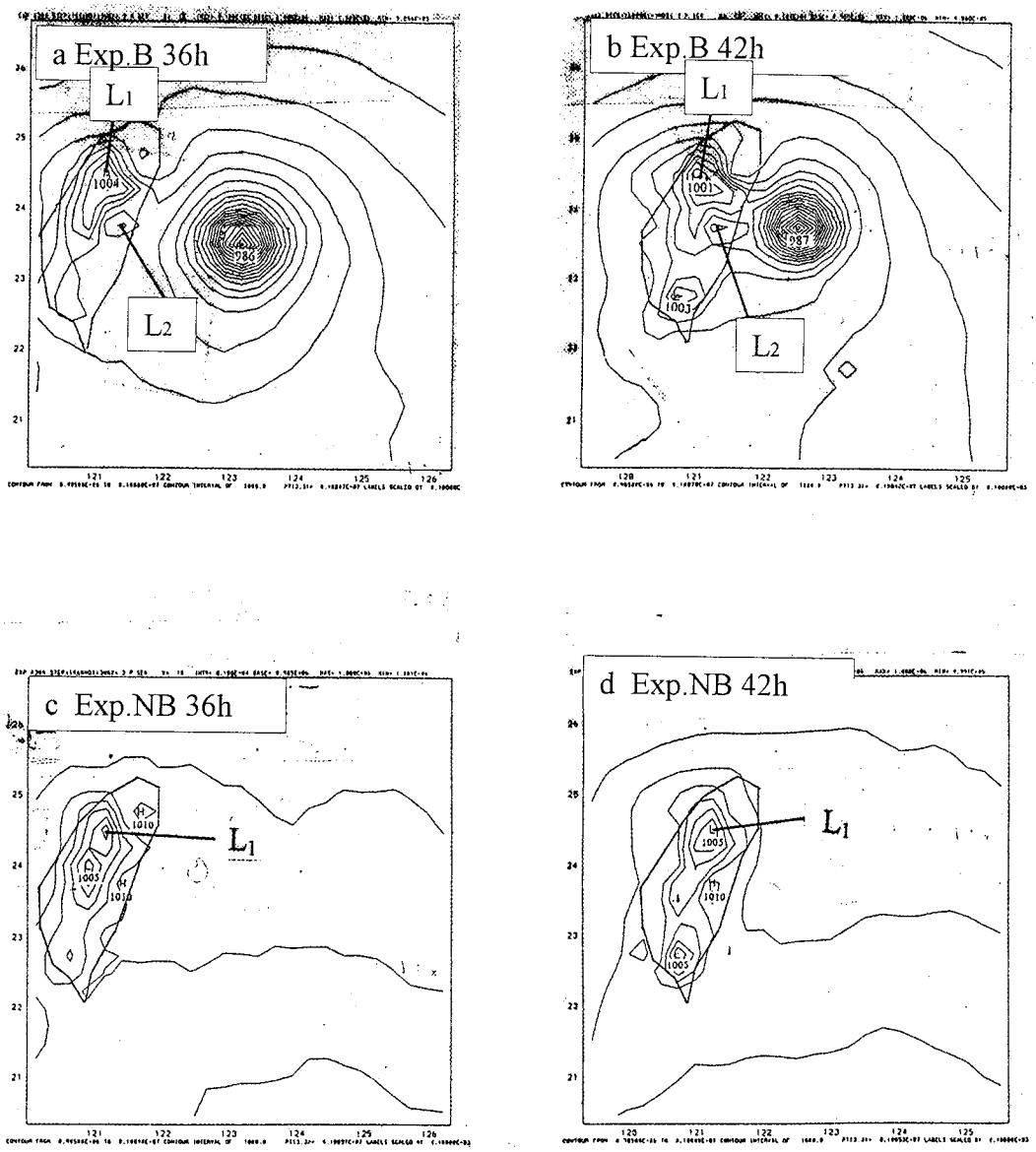

FIG. 9. Sea level pressure (in hPa) at (a) 36 and (b) 42 h from expt B; (c) and (d) same as in (a) and (b) but from expt NB.

rainfall over northeastern Taiwan (e.g., accumulated rainfall of 150 mm at Su-Au) and overpredicting the rainfall over southern Taiwan (likely to be related to the track being too far south), the model roughly captures the pattern of heavy precipitation over central Taiwan. The model simulates three local rainfall maxima (with the maximum value being 240 mm) around the three model-resolved mountain peaks, as compared to a maximum rainfall of 210 mm near Nio-Dray Mountain in central Taiwan. These differences may be partly due to the inadequate model resolution used to describe the complicated topography pattern over the CMR (cf. Figs. 10a and 10b), and partly due to the insufficient density of rain gauge stations for fully measuring the detailed precipitation distribution over the mountainous area in central Taiwan. As indicated in Wu and Kuo (1999), although the rainfall distribution for typhoons affecting Taiwan is often phase-locked with the Taiwan terrain, giving the uncertainty in simulating the landfall location and typhoon intensity, the mesoscale precipitation distribution associated with a typhoon landfalling in Taiwan remains a big challenge for all numerical models.

3) PV BUDGET

To obtain more insight on the role of advective, diabatic, and frictional processes in affecting the storm evolution, the PV budget is calculated here based on

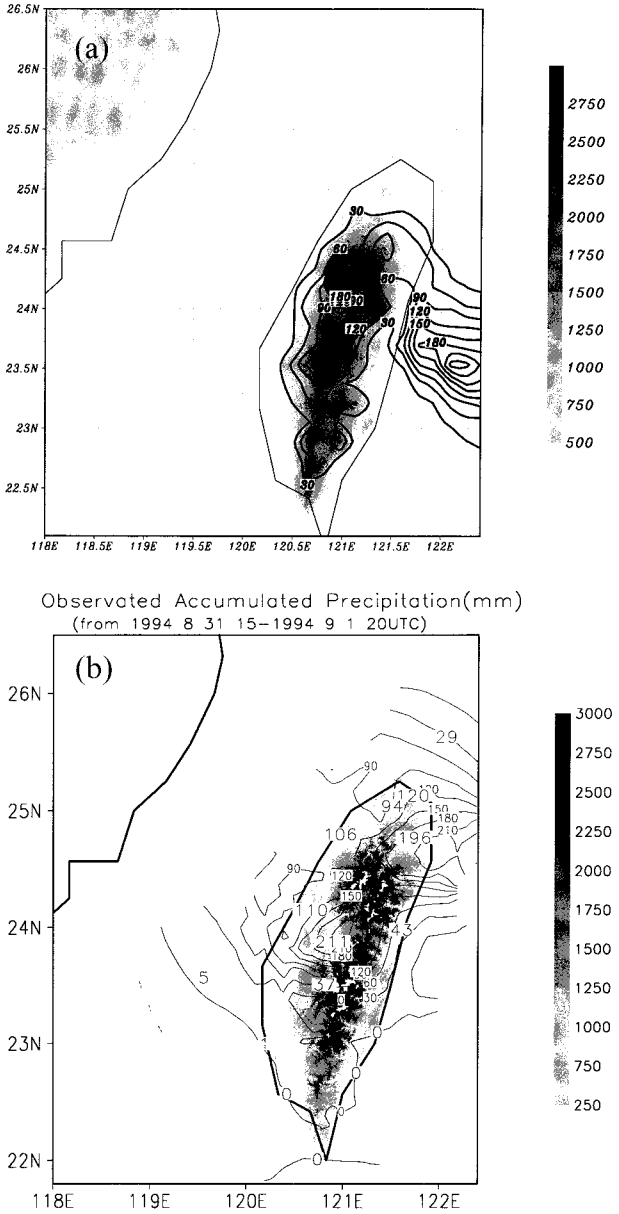

FIG. 10. (a) Simulated accumulated precipitation (contour interval of 30 mm) and the model terrain (shading with interval of 500 m) from 36 to 54 h (0000–1800 UTC 1 Sep 1994) in the finest mesh from the control experiment (expt B); (b) same as in (a) but for observed precipitation and actual terrain data with 30-s resolution.

the same formulation as by Wu and Kurihara (1996); that is, we formulate our calculation of the PV budget on the π coordinate [Exner function: $\pi = C_p(p/p_0)^\kappa$]. The approximate definition of Ertel's PV in π coordinates is

$$q = -\frac{g\kappa\pi}{p}\left(\eta\frac{\partial\theta}{\partial\pi} - \frac{1}{a\cos\varphi}\frac{\partial v}{\partial\pi}\frac{\partial\theta}{\partial\lambda} + \frac{1}{a}\frac{\partial u}{\partial\pi}\frac{\partial\theta}{\partial\varphi}\right),$$

where $\kappa = R_d/C_p$, p is the pressure, η is the vertical component of absolute vorticity, and θ is the potential temperature. The PV budget is

$$\frac{\partial q}{\partial t} = -\mathbf{v}_h\cdot\nabla_h q - \omega^*\frac{\partial q}{\partial\pi} + \frac{g\kappa\pi}{p}\left[\boldsymbol{\eta}\cdot\nabla\left(\frac{d\theta}{dt}\right) + \nabla\theta\cdot\nabla\times\boldsymbol{F}\right],$$

where $\omega^* \equiv d\pi/dt$, and the terms on the right represent the local change of PV due to the horizontal and vertical advection, and the effect from diabatic heating ($d\theta/dt$, including the condensational and radiative heating) and friction ($\mathbf{F}$), respectively. It should be noted that the analysis may reduce numerical accuracy due to the interpolation from the model's sigma coordinate to the π coordinate. However, as will be shown later, the effect from both the vertical motion and condensational heating is predominent in the inner part of Gladys. It is anticipated that the effects due to the above terms are predominant in the PV budget analysis in any of the π, sigma, or θ coordinates. It can be assumed that a major feature of the PV budget is captured from this analysis.

At 36 h, the distribution of condensational heating (Fig. 11a) is consistent with that of upward motion (Fig. 5b). The result suggests that the condensation occurs mainly on the resolvable scale in the model since we have also conducted simulations with the cumulus parameterization turned off, and have produced similar heating profiles. (No absolute convective instability occurs in these no-convective-adjustment simulations, probably due to the effect of strong vertical mixing within the vortex.) The maximum condensational heating (about 65 K h^{-1}) occurred on the western flank of the eyewall at about 650 mb, while the values for the eastern flank were 60 K h^{-1} at 400 mb. This condensational heating profile causes the redistribution of PV in the vertical direction (Fig. 11b) by creating a negative PV anomaly in the upper troposphere [at a rate of about -4 PVU $(12\ h)^{-1}$ at 350 mb] and a positive PV anomaly in the lower troposphere [8 PVU $(12\ h)^{-1}$ at 600 mb].

In the entire troposphere, there is a very weak positive horizontal PV advection to the downshear side of Gladys, and a very weak negative one to the upshear side (figures not shown). This horizontal PV advection is much weaker compared to those terms associated with the condensational heating. The local change in the PV tendency due to the vertical advection (Fig. 11c) is strongest at Gladys's center. Physically, the strong updraft near the hurricane center carries the high-PV air from the middle troposphere to the upper troposphere and the low-PV air from the lower troposphere to the middle troposphere, thus producing a maximum positive PV tendency of 1 PVU $(12\ h)^{-1}$ at about the 350-mb level, and a negative PV tendency [about -0.3 PVU $(12\ h)^{-1}$] in the lower and middle troposphere. The frictional effect on PV is very small (Fig. 11d), and is

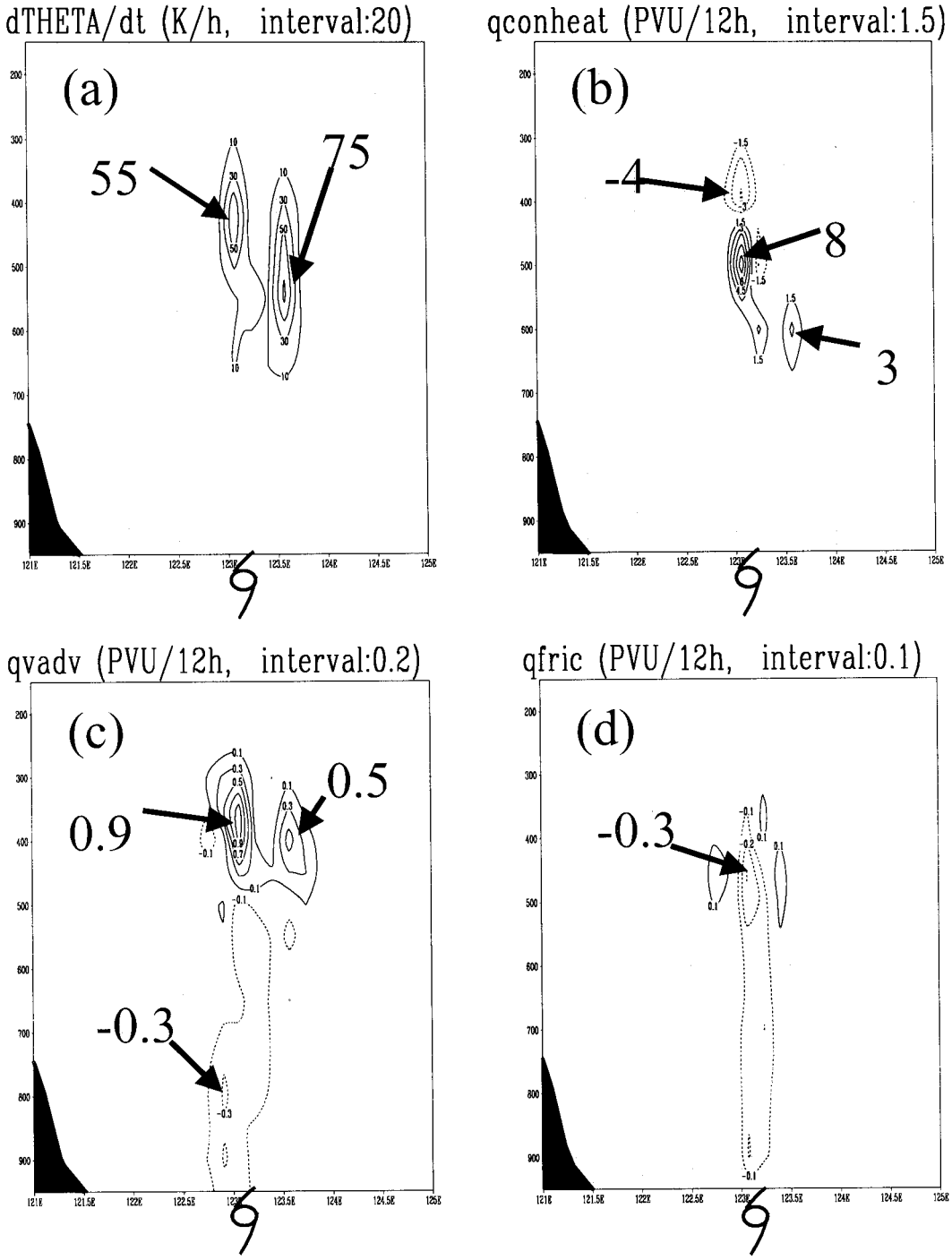

FIG. 11. (a) West–east cross section, cutting through the storm center, of the condensational heating rate (contour interval of 20 K h^{-1}) at 36 h from the control experiment (expt B); west–east cross section of the change of potential vorticity due to (b) condensational heating [contour interval of 1.5 PVU $(12\ h)^{-1}$], (c) vertical advection [contour interval of 0.2 PVU $(12\ h)^{-1}$], and (d) friction [contour interval of 0.1 PVU $(12\ h)^{-1}$]. The bold solid line indicates the topography of Taiwan.

mainly present near the hurricane center, where large horizontal wind shear exists.

Our calculation clearly shows that the local change in PV due to other nonconservative processes (including both the radiative heating and friction) is more than an order of magnitude smaller than that due to the condensational heating. In other words, condensational heating is the primary nonconservative factor affecting Gladys's PV evolution. The local change of PV due to all terms (figure not shown), including the total advection, heating, and friction, indicates that there existed a PV source in the middle to lower troposphere, and a sink in the upper troposphere at Gladys's center.

Similar results are also found at other forecast times before landfall. For example, at 42 h the condensational heating term indicated a 35 K h^{-1} heating rate (Fig. 12a) at about 400 mb, which is associated with the updraft on the western side of the storm center. Such heating results in a PV sink of -2 PVU (12 h)$^{-1}$ at 350 mb and a PV source of 3.5 PVU (12 h)$^{-1}$ at 550 mb (Fig. 12b). The vertical advection of PV still shows an upward transportation of PV air and, thus, leads to a PV tendency of 1 PVU (12 h)$^{-1}$ at 400 mb, -0.8 PVU (12 h)$^{-1}$ at 650 mb, and -0.4 PVU (12 h)$^{-1}$ at 800 mb. The frictional effect remains insignificant (Fig. 12d) even though Gladys is near the Taiwan terrain.

Once Gladys is already located inland over Taiwan (e.g., at 48 h in Fig. 13), strong condensational heating is still found over the mountains, with a peak heating rate reaching 80 K h^{-1} at 500 mb (Fig. 13a), which is consistent with the distribution of the vertical velocity. However, because of the disintegration of the PV structure (Fig. 7a) over the terrain, the PV change due to condensational heating (Fig. 13b) is quite different from the typical dipole patterns (positive tendency below and negative above) found in earlier hours (cf. Figs. 11b and 12b). The pattern of upward transport of high-PV air seen in Figs. 11c and 12c is not found in Fig. 13c. Meanwhile, Fig. 13d indicates that the frictional effect becomes larger and results in PV tendencies of -2 PVU (12 h)$^{-1}$ (about the same order of magnitude as the other processes) both near the surface and at about 350 mb. As a result, the net PV tendency due to all processes shows a complicated pattern (figure not shown). The result suggests that the detailed PV redistribution processes are more complicated for a storm, such as Gladys, which made landfall over Taiwan terrain, than for the oceanic storms, for example, Hurricane Bob (1991) in Wu and Kurihara (1996). Note that our analysis shows that some frictional dissipation of PV exists over the surface (e.g., Fig. 13d), and can significantly affect the PV evolution of Gladys after its landfall. It is well recognized that a tropical storm decays quickly after making landfall, mainly due to the cutoff of water vapor supply from ocean, as well as the effect of the friction-induced Ekman spindown process. Our analysis provides a PV view of the frictional effect on a landfalling typhoon, even though the direct mechanical effect of the surface drag on the momentum budget is not estimated separately.

Overall, the PV budget analysis clearly demonstrates that vertical advection and the effect of condensational heating are the two dominant processes causing the local change in PV for Gladys. However, when compared with the PV budget analysis of Hurricane Bob (1991) in Wu and Kurihara (1996), some differences are found. First, as Gladys is a much weaker storm, it appears that the PV tendency due to vertical advection is weaker, and cannot compensate for the stronger PV redistribution due to the condensational effect; second, the PV distribution near the storm center over the topography is less organized than that over the ocean, and thus even though the model demonstrates strong updraft and condensational heating in the eyewall region, the PV budget appears to be very noisy. The result indicates the difficulty in interpreting the PV budget when the storms are over the mountains. Nevertheless, consistent with Wu and Kurihara (1996) is that our results also indicate that the diabatic heating effect plays a crucial role in the evolution of the PV field in typhoons. It also suggests the importance of accurate representation of the heating profile in typhoon models when the storm encounters topography. Finally, it should be stressed that because any new eddy from PV generation may lead to the track deflection or affect the storm development, more case studies and more detailed analyses are needed in order to better understand the dynamics of the effect of the Taiwan terrain on typhoons based on PV budget analysis.

c. Sensitivity experiments

1) EXPERIMENT NT

Comparing the control experiment (expt B) with experiment NT, in which the Taiwan topography is removed, it is clear that the presence of the topography results in the deceleration of Gladys's translation speed from 27 to 39 h, and then its acceleration from 39 to 46 h as it approached Taiwan (Fig. 14a). Decomposition of the storm movement into the zonal velocity (Fig. 14b) and meridional velocity (Fig. 14c) indicates that when Gladys is about 300 to 200 km away from Taiwan (27–39 h), the deceleration due to the presence of the Taiwan terrain is mainly on the zonal speed, which is consistent with the result of zonal deceleration at region B as indicated in Fig. 27 of Yeh and Elsberry (1993a). As shown in Fig. 8b, the northeasterly boundary flow associated with Gladys is blocked at the northeast coast of Taiwan, and some deflected and reversed flow inland of northeastern Taiwan is also found. Therefore we believe that the zonal deceleration should be principally associated with the barrier blocking (Wang 1980; Lin et al. 1999) of the background mean flow. Small southward deviation (Fig. 14c) also exists between 12 and 33 h, which is consistent with Yeh and Elsberry

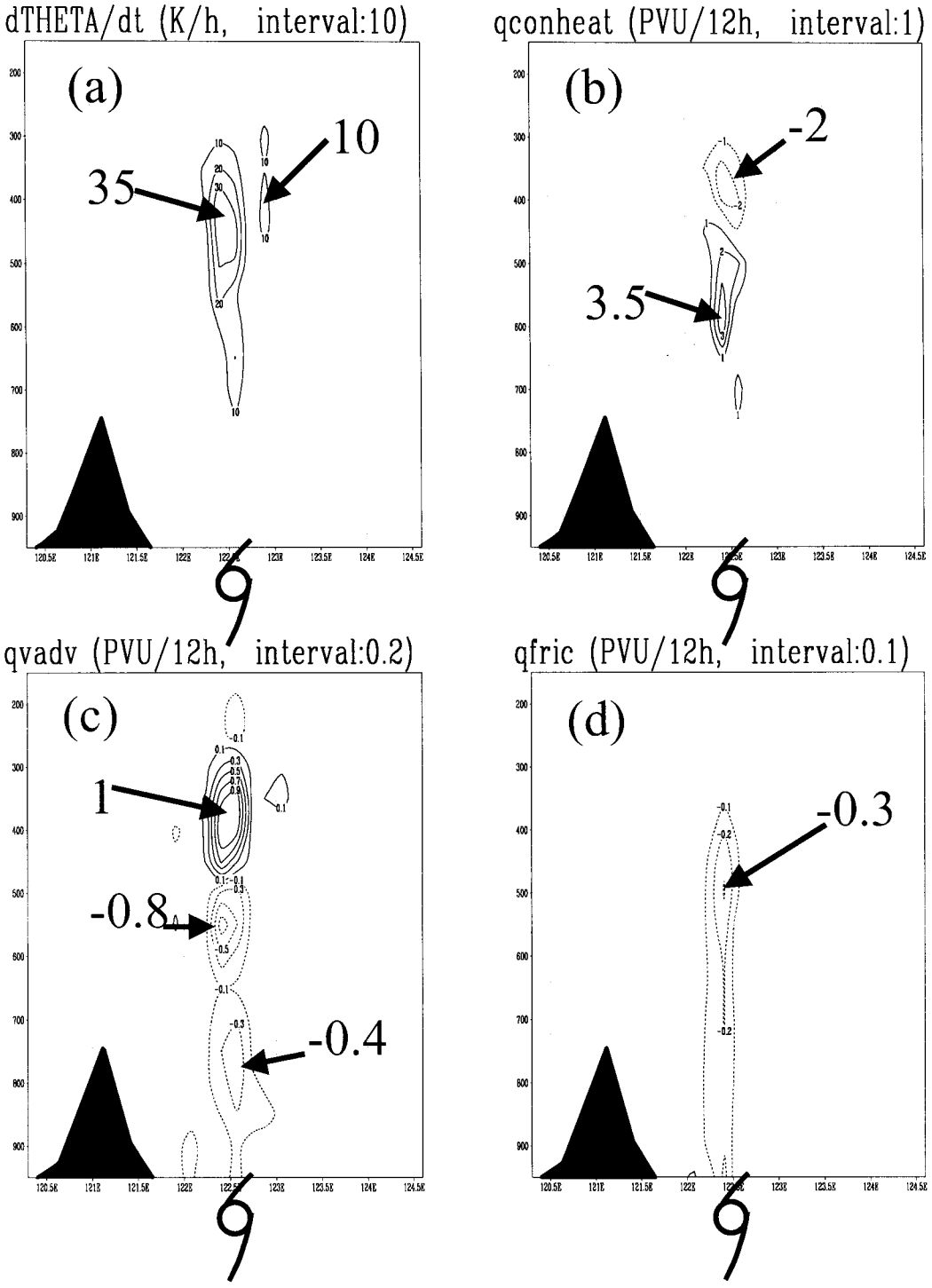

FIG. 12. (a) West–east cross section, cutting through the storm center, of the condensational heating rate (contour interval of 10 K h^{-1}) at 42 h from the control experiment (expt B); west–east cross section of the change of potential vorticity due to (b) condensational heating [contour interval of 1 PVU $(12\ h)^{-1}$], (c) vertical advection [contour interval of 0.2 PVU $(12\ h)^{-1}$], and (d) friction [contour interval of 0.1 PVU $(12\ h)^{-1}$]. The bold solid line indicates the topography of Taiwan.

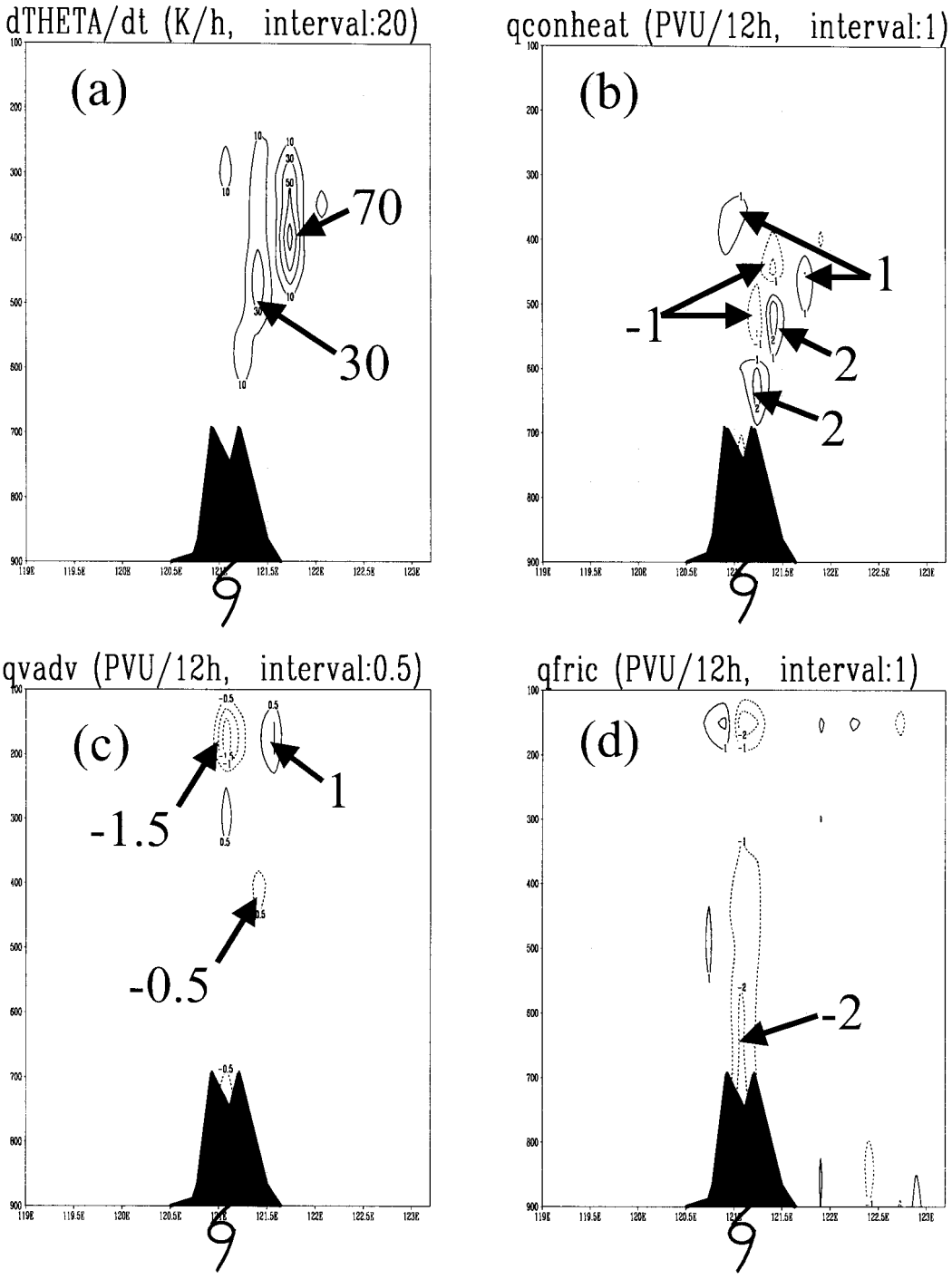

FIG. 13. (a) West–east cross section, cutting through the storm center, of the condensational heating rate (contour interval of 20 K h^{-1}) at 48 h from the control experiment (expt B); west–east cross section of the change of potential vorticity due to (b) condensational heating [contour interval of 1 PVU $(12\ h)^{-1}$], (c) vertical advection [contour interval of 0.5 PVU $(12\ h)^{-1}$], and (d) friction [contour interval of 1 PVU $(12\ h)^{-1}$]. The bold solid line indicates the topography of Taiwan.

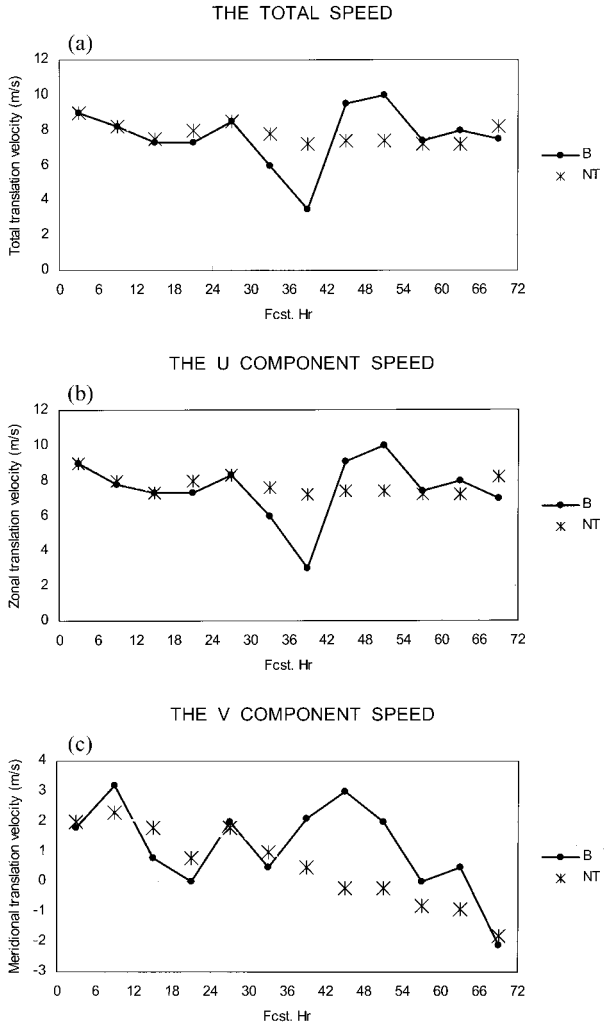

FIG. 14. The translation velocity of Gladys in expts B (solid) and NT (dashed): (a) total velocity, (b) zonal velocity, and (c) meridional velocity.

(1993a,b), though no explanation was given then. A possible mechanism for such southward deviation is the so-called channeling effect in which the air is forced southward by the ageostrophic pressure gradient when the storm circulation impinges on the topography (e.g., Huang and Lin 1997; Lin et al. 1999).

When the storm is within 100 km of Taiwan (i.e., from 39 to 46 h), both the zonal and meridional translation speed increased, thus leading to a northwestward track, which is in agreement with the statistics of Wang (1980), and the result of Chang (1982), Bender et al. (1987), and Yeh and Elsberry (1993a,b). Note that the magnitude of acceleration in this case is smaller than that in Chang (1982) and Bender et al. (1987), which is likely to be because Gladys is originally moving at an average speed of 8 m s^{-1}, which is faster than the 5 m s^{-1} background flow used in both Chang (1982) and Bender et al. (1987). Bender et al. (1987) argued that the storm is advected by the accelerated mean flow due to the influence of the topogaphy on the mean flow and the extra southerly flow induced by the interaction of the storm circulation with the topography, though further explanation on why this occurred was not discussed.

In the simulation of a vortex passing a bell-shaped topography under a uniform background flow (Lin et al. 1999, see their Fig. 13), the vortex deviated southward before landfall, then turned northward after passing the central axis of the topography. This track pattern is consistent with the response of an idealized flow over an isolated topography on the f plane (Peng et al. 1995). It is interesting to ask why our model track turned northward before landfall, instead of after passing the central axis of the terrain, as found in Lin et al. (1999). One likely answer is that this is related to the moist dynamics. Note that Lin et al. (1999) used a dry model without considering the moisture effect. In our full-physics simulation, right before landfall (e.g., 42 h), the upslope lifting of the moisture-laden air produces heavy precipitation (see Fig. 10a) over the northwest quadrant of Gladys. Meanwhile, to the southwest of Gladys, as shown in Fig. 8b, downslope dry air is dominant, which tends to inhibit the development of convective activity. Therefore, the moist dynamics appears to play an important role in favoring new convection and diabatically generating potential vorticity to the northwest quadrant of Gladys. We believe such an asymmetric feature can lead to a different storm track as compared to the theoretical result from the dry model. Our reasoning above appears to fill the gap in interpreting the inconsistency between Bender et al. (1987) and Lin et al. (1999).

As to the intensity simulation (Fig. 2), the control experiment (expt B) indicates rapid weakening after 36 h as Gladys approaches and makes landfall on Taiwan. Meanwhile, experiment NT (with no topography) indicates that the intensity of Gladys remains the same as that in experiment B up to 36 h. After 36 h, the intensity of NT remains at 65 kt for another 18 h until 54 h, 3 h before landfall in southern China. Without the drying effect or the topographic blocking shown in the control experiment, experiment NT thus simulates a storm of sustained intensity while passing Taiwan with flat terrain.

2) EXPERIMENT B2

The last experiment (B2), with a stronger and larger bogus vortex, shows that the motion of such a vortex is affected by a stronger beta effect (Fiorino and Elsberry 1989) and, thus, leads to a more northwestward track (Fig. 1) and does not make landfall on Taiwan. As such, the resulting wind and precipitation distribution is significantly different from the control experiment. Nevertheless, the motion of the B2 vortex is clearly affected by the Taiwan terrain and makes a distinct cyclonic turn as it passes through the region offshore from northern Taiwan. The above result indicates that

the improper specification of the typhoon vortex in the model can affect the track forecast significantly, especially when the typhoon vortex encounters high terrain. Therefore, accurate representation of the typhoon vortex is needed to understand the typhoon–topography interaction problem.

4. Summary

A real-case simulation of Typhoon Gladys (1994) using the GFDL hurricane prediction system is presented in this paper to evaluate the model capability in simulating the track, intensity, and mesoscale features of Gladys under the influence of the Taiwan terrain. To study the impact of the CMR on the evolution of Gladys, experiments were also performed, with or without the Taiwan terrain, and with or without the typhoon vortex of different strengths. The control numerical experiment shows a fairly accurate track simulation for Gladys, especially during the first 54 h. Consistent with most previous studies, the Taiwan topography results in the deceleration of Gladys's translation speed and southward deviation as it approaches Taiwan. On the other hand, Gladys accelerates northwestward while passing Taiwan, which is likely to be related to the moist processes, as compared to the different track pattern in the dry model of Lin et al. (1999). Although the GFDL hurricane model forecast underestimates Gladys's intensity, the model captures the evolution of Gladys's intensity, especially the weakening of Gladys during landfall. The mesoscale phenomena, including the pattern of heavy precipitation and the formation of secondary lows, are also well simulated by the model, though their locations are somewhat different from the observations. This inconsistency is probably related to the limitation of the model resolution in resolving the complicated terrain over Taiwan, and the model's capability in simulating the storm intensity.

Comparison of different experiments indicates that the surface low pressure center to the east of the CMR is induced by the downslope adiabatic warming (foehn) associated with the circulation of Gladys. The quasi-stationary secondary low to the west of the CMR is mainly induced by the environmental easterly flow over the CMR, while the downslope adiabatic warming associated with the circulation of Gladys acts to enhance it as Gladys was close to Taiwan. The potential vorticity budget analysis indicates that the condensational heating plays a major role in the potential vorticity evolution around the storm. Note that the surface frictional dissipation of the potential vorticity becomes more significant as Gladys is over the Taiwan terrain. It is shown that potential vorticity evolution over the terrain is much more complicated compared to that associated with storms over the ocean. Finally, the experiment with a larger and stronger initial typhoon vortex indicates that a different initial specification of the typhoon vortex can result in a different track pattern and thus leads to a totally different typhoon–topography interaction, suggesting the importance of typhoon initialization for storm prediction near Taiwan.

It is suggested that to improve the ability to simulate the evolution of typhoons near Taiwan and their associated mesoscale wind and precipitation distributions, and to better understand the dynamics of the detailed typhoon–topography interaction, improved observations need to be incorporated into high-resolution numerical models through advanced data assimilation techniques. It is hoped that an interplay between high-resolution numerical assimilation and mesoscale analyses could offer much new insight into the problems of typhoons affected by the Taiwan terrain. Further study using a nonhydrostatic mesoscale model (the Pennsylvania State University–National Center for Atmospheric Research fifth-generation Mesoscale Model) with a higher resolution (6.7 km compared to the 19-km resolution in this paper), and with the capability for assimilating other special data (such as satellite wind and precipitable water), will be presented in a follow-up paper.

Acknowledgments. The author thanks Yoshio Kurihara and Morris Bender for their kind help on the use of the GFDL hurricane model. I appreciate the valuable comments from the anonymous reviewers, which led to a great improvement of this paper. Helpful discussions with Yuh-Lang Lin, Richard Rotunno, Chris Davis, Hung-Chi Kuo, Ching-Yuang Huang, Tien-Chuan Yeh, and Shi-Ting Wang are appreciated. I also thank Yu-Tseng Cho and Tzu-Hsiung Yen for their assistance on the graphics. This work is supported through the National Science Council of Taiwan by Grants NSC86-2111-M-002-009-AP1, NSC87-2111-M-002-004-AP1, and NSC88-2111-M-002-004-AP1.

REFERENCES

Bender, M. A., and I. Ginis, 2000: Real case simulations of hurricane–ocean interaction using a high-resolution coupled model: Effects on hurricane intensity. *Mon. Wea. Rev.*, **128,** 917–946.

——, R. E. Tuleya, and Y. Kurihara, 1985: A numerical study of the effect of a mountain range on a landfalling tropical cyclone. *Mon. Wea. Rev.*, **113,** 567–582.

——, ——, and ——, 1987: A numerical study of the effect of island terrain on tropical cyclones. *Mon. Wea. Rev.*, **115,** 130–155.

——, R. J. Ross, R. E. Tuleya, and Y. Kurihara, 1993: Improvements in tropical cyclone track and intensity forecasts using the GFDL initialization system. *Mon. Wea. Rev.*, **121,** 2046–2061.

Brand, S., and J. W. Blelloch, 1974: Changes in the characteristics of typhoons crossing the island of Taiwan. *Mon. Wea. Rev.*, **102,** 708–713.

Chang, S. W., 1982: The orographic effects induced by an island mountain range on propagating tropical cyclones. *Mon. Wea. Rev.*, **110,** 1255–1270.

Dong, K., and C. J. Neumann, 1986: The relation between tropical cyclone motion and environmental geostrophic flows. *Mon. Wea. Rev.*, **114,** 115–122.

Fiorino, M., and R. L. Elsberry, 1989: Some aspects of vortex structure related to tropical cyclone motion. *J. Atmos. Sci.*, **46,** 975–990.

Huang, C.-Y., and Y.-L. Lin, 1997: The evolution of mesoscale vortex impinging on symmetric topography. *Proc. Taiwan Natl. Sci. Counc.,* **21A,** 285–309.
——, and Y.-P. Hsu, 1998: The influence of Taiwan topography on the variation of idealized typhoon circulation (in Chinese with English abstract). *Atmos. Sci.,* **26,** 281–324.
Kurihara, Y., 1973: A scheme of moist convective adjustment. *Mon. Wea. Rev.,* **101,** 547–553.
——, and M. A. Bender, 1980: Use of a movable nested mesh model for tracking a small vortex. *Mon. Wea. Rev.,* **108,** 1792–1809.
——, C. L. Kerr, and M. A. Bender, 1989: An improved numerical scheme to treat the open lateral boundary of a regional model. *Mon. Wea. Rev.,* **117,** 2714–2722.
——, M. A. Bender, R. E. Tuleya, and R. Ross, 1990: Prediction experiments of Hurricane Gloria (1985) using a multiply nested movable mesh model. *Mon. Wea. Rev.,* **118,** 2185–2198.
——, ——, and R. J. Ross, 1993: An initialization scheme of hurricane models by vortex specification. *Mon. Wea. Rev.,* **121,** 2030–2045.
——, ——, R. E. Tuleya, and R. J. Ross, 1995: Improvements in the GFDL hurricane prediction system. *Mon. Wea. Rev.,* **123,** 2791–2801.
——, ——, and ——, 1998: The GFDL hurricane prediction system and its performance in the 1995 hurricane season. *Mon. Wea. Rev.,* **126,** 1306–1322.
Lacis, A. A., and J. E. Hansen, 1974: A parameterization for the absorption of solar radiation in the earth's atmosphere. *J. Atmos. Sci.,* **31,** 118–133.
Lin, Y.-L., N.-H. Lin, and R. P. Weglarz, 1992: Numerical modeling studies of lee mesolows, mesovortices, and mesocyclones with application to the formation of Taiwan mesolows. *Meteor. Atmos. Phys.,* **49,** 43–67.
——, J. Han, D. W. Hamilton, and C.-Y. Huang, 1999: Orographic influence on a drifting cyclone. *J. Atmos. Sci.,* **56,** 534–562.
Mellor, G. L., and T. Yamada, 1974: A hierarchy of turbulence closure models for planetary boundary layers. *J. Atmos. Sci.,* **31,** 1791–1806.
Peng, M. S., S.-W. Li, S. W. Chang, and R. T. Williams, 1995: Flow over mountains: Coriolis force, transient troughs and three dimensionality. *Quart. J. Roy. Meteor. Soc.,* **121,** 593–613.
Ross, R. J., and Y. Kurihara, 1992: A simplified scheme to simulate asymmetries due to the beta effect in barotropic vortices. *J. Atmos. Sci.,* **49,** 1620–1628.
Rotunno, R., V. Grubisic, and P. K. Smolarkiewicz, 1999: Vorticity and potential vorticity in mountain wakes. *J. Atmos. Sci.,* **56,** 2796–2810.
Schar, C., and R. B. Smith, 1993a: Shallow-water flow past isolated topography. Part I: Vorticity production and wake formation. *J. Atmos. Sci.,* **50,** 1373–1400.
——, and ——, 1993b: Shallow-water flow past isolated topography. Part II: Transition to vortex shedding. *J. Atmos. Sci.,* **50,** 1401–1412.
——, and D. R. Durran, 1997: Vortex formation and vortex shedding in continuously stratified flow past isolated topography. *J. Atmos. Sci.,* **54,** 534–554.
Schwarzkopf, M. D., and S. B. Fels, 1991: The simplified exchange method revisited: An accurate, rapid method for computation of infrared cooling rates and fluxes. *J. Geophys. Res.,* **96,** 9075–9096.
Shieh, S.-L., S.-T. Wang, M.-D. Cheng, and T.-C. Yeh, 1996: User's guide (1) for typhoon forecasting in the Taiwan area (in Chinese). Res. Rep. CWB84-1M-01, 356 pp.
Smith, R. B., 1979: The influence of mountains on the atmosphere. *Advanced in Geophysics,* Vol. 21, Academic Press, 87–230.
——, 1980: Linear theory of stratified hydrostatic flow past an isolated mountain. *Tellus,* **32,** 348–364.
——, 1989: Comments on ''Low Froude number flow past three-dimensional obstacles. Part I: Baroclinically generated lee vortices.'' *J. Atmos. Sci.,* **46,** 3611–3613.
——, and D. F. Smith, 1995: Pseudoinviscid wake formation by mountains in shallow-water flow with drifting vortex. *J. Atmos. Sci.,* **52,** 436–454.
Smolarkiewicz, P. K., and R. Rotunno, 1989: Low Froude number flow past three-dimensional obstacles. Part I: Baroclinically generated lee vortices. *J. Atmos. Sci.,* **46,** 1154–1164.
Sun, W.-Y., and J. D. Chern, 1994: Numerical experiments of vortices in the wakes of large idealized mountains. *J. Atmos. Sci.,* **51,** 191–209.
——, ——, C.-C. Wu, and W.-R. Hsu, 1991: Numerical simulation of mesoscale circulation in Taiwan and surrounding area. *Mon. Wea. Rev.,* **119,** 2558–2573.
Tuleya, R. E., 1994: Tropical storm development and decay: Sensitivity to surface boundary conditions. *Mon. Wea. Rev.,* **122,** 291–304.
——, M. A. Bender, and Y. Kurihara, 1984: A simulation study of the landfall of tropical cyclones using a movable nested-mesh model. *Mon. Wea. Rev.,* **112,** 124–136.
Wang, S.-T., 1980: Prediction of the behavior and strength of typhoons in Taiwan and its vicinity. Res. Rep. 108, National Science Council, Taipei, Taiwan, 100 pp.
——, 1989: Observational analysis of the orographically induced disturbances during TAMEX. *Workshop on TAMEX Preliminary Scientific Results,* Taipei, Taiwan, National Science Council, 279–286.
Wu, C.-C., and Y. Kurihara, 1996: A numerical study of the feedback mechanisms of hurricane–environment interaction on hurricane movement from the potential vorticity perspective. *J. Atmos. Sci.,* **53,** 2264–2282.
——, and Y.-H. Kuo, 1999: Typhoons affecting Taiwan: Current understanding and future challenges. *Bull. Amer. Meteor. Soc.,* **80,** 67–80.
——, Y.-T. Cho, and S.-T. Wang, 1999a: The effect of Taiwan terrain on Typhoon Gladys (1994). Part I: Observational study (in Chinese with English abstract). *Atmos. Sci.,* **27,** 1–28.
——, ——, and T.-H. Yen, 1999b: The effect of Taiwan terrain on Typhoon Gladys (1994). Part II: Numerical simulation (in Chinese with English abstract). *Atmos. Sci.,* **27,** 29–60.
——, M. A. Bender, and Y. Kurihara, 2000: Typhoon forecast with the GFDL hurricane model: Forecast skill and comparison of predictions using AVN and NOGAPS global analyses. *J. Meteor. Soc. Japan,* **78,** 777–788.
Yeh, T.-C., and R. L. Elsberry, 1993a: Interaction of typhoons with the Taiwan orography. Part I: Upstream track deflections. *Mon. Wea. Rev.,* **121,** 3193–3212.
——, and ——, 1993b: Interaction of typhoons with the Taiwan orography. Part II: Continuous and discontinuous tracks across the island. *Mon. Wea. Rev.,* **121,** 3213–3233.